Macromolecules

pubs.acs.org/Macromolecules Article

Controlling n-Type Molecular Doping *via* Regiochemistry and Polarity of Pendant Groups on Low Band Gap Donor–Acceptor Copolymers

Gang Ye, Jian Liu,* Xinkai Qiu, Sebastian Stäter, Li Qiu, Yuru Liu, Xuwen Yang, Richard Hildner, L. Jan Anton Koster,* and Ryan C. Chiechi*

Cite This: *Macromolecules* 2021, 54, 3886–3896 Read Online

ACCESS | Metrics & More | Article Recommendations | Supporting Information

ABSTRACT: We demonstrate the impact of the type and position of pendant groups on the n-doping of low-band gap donor–acceptor (D–A) copolymers. Polar glycol ether groups simultaneously increase the electron affinities of D–A copolymers and improve the host/dopant miscibility compared to nonpolar alkyl groups, improving the doping efficiency by a factor of over 40. The bulk mobility of the doped films increases with the fraction of polar groups, leading to a best conductivity of 0.08 S cm^{-1} and power factor (PF) of 0.24 μW m^{-1} K^{-2} in the doped copolymer with the polar pendant groups on both the D and A moieties. We used spatially resolved absorption spectroscopy to relate commensurate morphological changes to the dispersion of dopants and to the relative local doping efficiency, demonstrating a direct relationship between the morphology of the polymer phase, the solvation of the molecular dopant, and the electrical properties of doped films. Our work offers fundamental new insights into the influence of the physical properties of pendant chains on the molecular doping process, which should be generalizable to any molecularly doped polymer films.

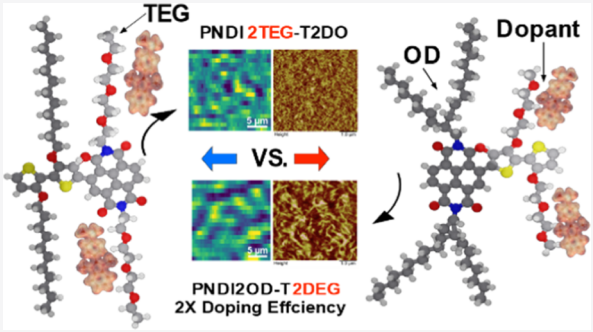

INTRODUCTION

The two primary synthetic handles for manipulating the properties of conjugated polymers are the backbone, for controlling the electronic structure, and the pendant groups, for controlling solubility and processing. Much of the conventional wisdom of structure–property relationships, however, derives from the performance of thin films of conjugated polymers in their pristine, undoped, semiconducting state, for example, photovoltaics and field-effect transistors. Thermoelectric devices exploit the difference in entropy that develops in response to a thermal gradient across a population of charge carriers. Molecular doping[1−7] (i.e., chemical doping with redox-active organic compounds) tends to be milder and more amenable to solution processing compared to other methods, as harsher dopants tend to render conjugated polymers insoluble. Thus, the development of (particularly n-type) conjugated polymers for thermoelectric applications requires developing synthetic strategies for optimizing both doping efficiency and the morphology of molecularly doped films.

The strategy for designing materials for organic thermoelectric devices is to modulate the carrier density by molecular doping to optimize the power factor (PF = $S^2\sigma$, where S and σ are the Seebeck coefficient and electrical conductivity, respectively).[8,9] Molecular doping can be accomplished by simply mixing the polymer and (pre)dopant, casting the mixture into a film, and annealing. However, relatively large organic dopants tend to disturb the packing of host (macro)molecules and degrade charge transport.[10] Thus, one design principle is to maximize doping efficiency to generate a high density of carriers with a minimal dopant. So far, many factors, such as the strength of the dopant, the morphology of the doped film, and the processing conditions, have been exploited to increase doping efficiency.[11−15] However, most studies have focused on p-doped organic semiconductors; the development of their n-type counterparts lags behind. Most n-type organic semiconductors possess high-lying lowest unoccupied molecular orbital (LUMO) levels (≥−4.0 eV), which impedes the development of air-stable n-type dopants and sufficiently high doping efficiency.

In their pioneering work on n-doping of solution-processed conjugated polymers, Chabinyc and co-workers reported a maximum electrical conductivity of 10^{-3} S cm^{-1} poly{[*N*,*N*′-bis(2-octyldodecyl)-naphthalene-1,4,5,8-bis(dicarboximide)-

Received: February 10, 2021
Revised: March 29, 2021
Published: April 8, 2021

https://doi.org/10.1021/acs.macromol.1c00317
Macromolecules 2021, 54, 3886–3896

Scheme 1. Synthetic Routes to the Copolymers and Chemical Structure of *n*-DMBI

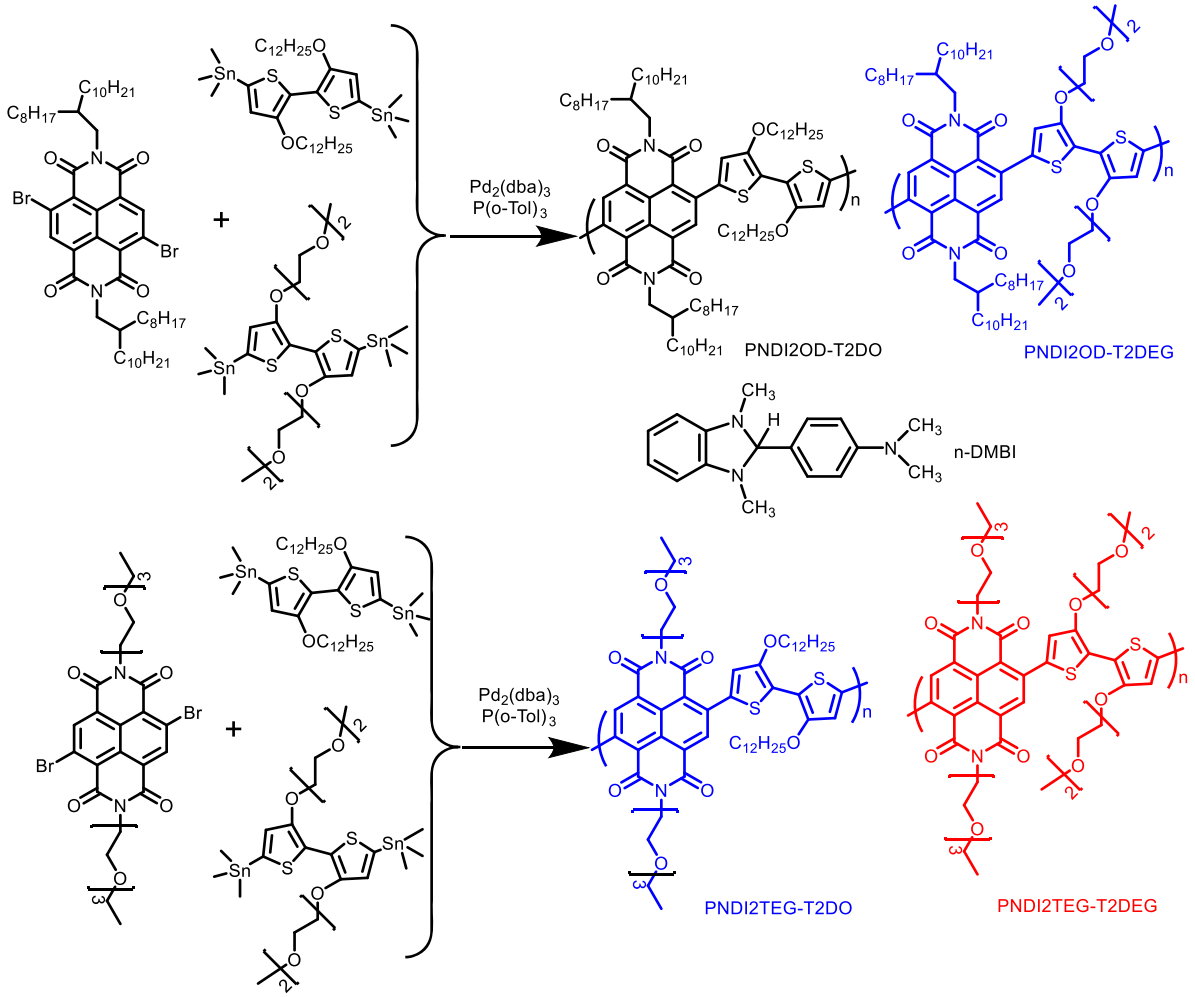

2,6-diyl]-*alt*-5,5′-(2,2′-bithiophene)} (PNDI2OD-T2) doped by (4-(1,3-dimethyl-2,3-dihydro-1*H*-benzoimidazol-2-yl)-phenyl)dimethylamine (*n*-DMBI).[10] Bao and co-workers systematically tuned the donor−acceptor (D−A) backbone structure and achieved a conductivity of 0.45 S cm^{-1}.[16] Pei and co-workers similarly modified the backbone of conjugated polymers to increase the charge mobility and doping level, leading to an even higher electrical conductivity of 14 S cm^{-1}.[17] Wang *et al.* furthered this trend, reporting a conductivity of 2.4 S cm^{-1} in n-doped poly(benzimidazole benzophenanthroline).[18] Recently, several groups, including ours, successfully utilized these insights into molecular doping to enhance the thermoelectric properties of doped D−A copolymers by using a weaker donor moiety.[19−21] Recently, Lei *et al.* reported a pyrazine-flanked diketopyrrolopyrrole polymer with a weak donor backbone structure that exhibits high n-type electrical conductivities of up to 8.4 S cm^{-1} and PF up to 57.3 μW m^{-1} K^{-2}.[22] Wang and Takimiya reported an acceptor−acceptor n-type copolymer consisting of naphthodithiophenediimide and bithiopheneimide building blocks, showing an impressive n-type conductivity value of up to 11.6 S cm^{-1} and PF up to 53.4 μW m^{-1} K^{-2}.[23] To the best of our knowledge, most of the previous work has focused exclusively on the effects of the backbones (i.e., the electronic structure) on n-doping of conjugated polymers, relegating modifications of the pendant groups to empirical observations about solubility and film formation; pendant groups affect the processing and packing of conjugated polymers, improving charge transport.[24,25] However, the interplay between pendant groups and molecular doping remains poorly understood. A better understanding of the unique role that pendant groups, particularly aliphatic chains, play in molecular doping is critical to maximizing the performance of organic thermoelectrics.

Recently, decorating n-type conjugated polymers with polar glycol ether pendant groups has drawn intensive attention for applications in organic thermoelectrics, as polar side chains promote the solubility of the dopant in the polymer matrix, thus enhancing the molecular doping efficiency.[26] Our group reported an n-type D−A copolymer with a backbone consisting of 2,6-dibromonaphthalene-1,4,5,8-tetracarboxylic diimide (NDI) and bithiophene (T2) moieties in which the NDI moiety is functionalized with the glycol ether side chains.[27] The molecular n-doping of this novel D−A copolymer achieved a 200-fold enhancement of electrical conductivity compared with analogues bearing aliphatic pendant groups. Giovannitti *et al.* reported a D−A copolymer with naphthalene diimide (NDI) and bithiophene (T2) backbone, where both D and A moieties are functionalized with the glycol ether side chains.[28] This copolymer features a very narrow band gap of 0.7 eV and a low-lying LUMO level of −4.12 eV and has been used in n-type organic electrochemical transistors to achieve *in operando* stability in water. The n-

https://doi.org/10.1021/acs.macromol.1c00317
Macromolecules 2021, 54, 3886−3896

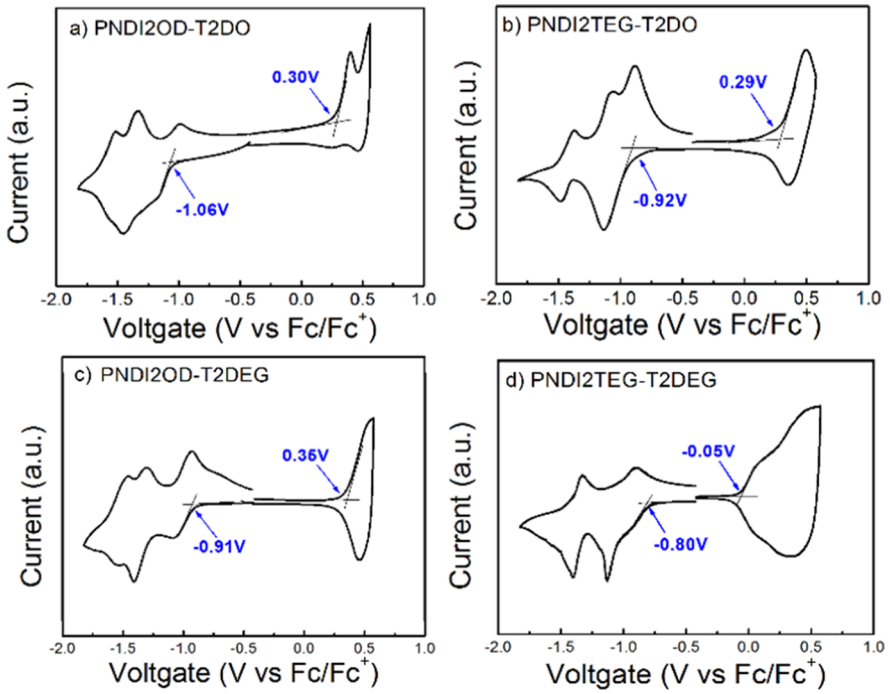

Figure 1. Cyclic voltammograms of the NDI-based conjugated polymer thin films deposited on the glass carbon working electrode immersed in 0.1 M *n*-Bu_4PF_6 acetonitrile solution at 100 mV s^{-1}. All four copolymers show quasi-reversible reduction and irreversible oxidation waves. Replacing pendant alkyl chains with polar glycol ethers has little effect on the oxidation potential, except when installed on both monomers, while the reduction potential systematically decreases with increasing glycol ether chains.

doping of this low-band gap copolymer has recently been reported by Müller and co-workers.[29] While glycol ether pendant groups are frequently employed to increase the polarity of films, the impact of their regiochemistry has not been studied. Thus, a comprehensive understanding of the effects of both the type and position of pendant groups on n-doping is indeed needed.

This paper describes the influence of the systematic alteration of the identity and regiochemistry of nonpolar-(izable) and polar(izable) pendant groups of the D−A copolymer backbone NDI-*alt*-T2 on molecular doping in thin films. We explored different combinations of alkyl and glycol ether pendant groups, synthesizing four D−A copolymers and studying their doping behaviors with varying concentrations of *n*-DMBI. We found that polar(izable) chains located on the D (bithiophene), A (napthalene diimide), or both monomers can almost equally improve the host/dopant miscibility and significantly increase the doping efficiency as compared to the baseline case of alkyl side chains on both. We found a maximum electrical conductivity of 0.08 S cm^{-1} and PF of 0.24 μW m^{-1} K^{-2} in the doped D−A copolymer with both monomers functionalized with glycol ether side chains, but that doping efficiency was influenced more by the relative positions of alkyl and glycol ether side chains. These changes in electrical properties were commensurate with large changes to film morphologies as inferred from atomic force microscope (AFM) topography. Using spatially resolved absorption spectroscopy (SRAS), we established a relationship between the topography and the solvation and dispersion of molecular dopants.

RESULTS AND DISCUSSION

The synthetic route and corresponding structures of the four D−A copolymers are shown in Scheme 1. The NDI-based monomers were synthesized and purified according to the previously reported procedures.[30] The bithiophene moiety was synthesized according to literature procedures with slight modifications (see the details in the Supporting Information).[31−33] The copolymers were synthesized by palladium-catalyzed Stille polycondensation of symmetrical dibromo and distannyl monomers. Full conversion to the respective polymers occurred after refluxing the degassed polymerization mixture overnight. Impurities and low-molecular weight fraction were removed by continuous extraction with hot methanol, followed by hexane and chloroform in a Soxhlet extractor. The crude polymer was then dissolved, precipitated into cold methanol, collected by centrifugation, and dried *in vacuo*. The structures were then characterized by ^{1}H NMR and Fourier-transform infrared spectroscopy (FT-IR) (Figures S1−S8, Supporting Information). The presence of glycol ether side chains was confirmed by the appearance and enhancement of the C−O−C stretching mode at 1109−1057 cm^{-1} in the FT-IR spectra of the polymers. The intensities of these absorptions increased consistently with the ratio of the glycol ether side chains. Finally, the relative molecular weights and polydispersities were determined by high-temperature gel permeation chromatography (GPC) in trichlorobenzene using a polystyrene standard. These data are summarized in Table S1.

The thermal properties of the copolymers were evaluated by thermogravimetric analysis and differential scanning calorimetry (DSC). The onset of decomposition (T_d) was determined from the temperature at 5% weight loss occurred. All the copolymers exhibited excellent thermal stability with T_d of 334, 321, 335, and 307 °C for PNDI2OD-T2DO, PNDI2TEG-T2DO, PNDI2OD-T2DEG, and PNDI2TEG-T2DEG, respectively (Figure S11, Supporting Information). These values of T_d are all sufficient for (thermoelectric) device application. The DSC curves of PNDI2TEG-T2DO and PNDI2OD-

https://doi.org/10.1021/acs.macromol.1c00317
Macromolecules 2021, 54, 3886−3896

Table 1. Photophysical Properties and Electrochemical Properties of NDI-Based Conjugated Polymers

polymer	PNDI2OD-T2DO	PNDI2TEG-T2DO	PNDI2OD-T2DEG	PNDI2TEG-T2DEG
$\lambda_{\text{sol. onset}}$ (nm)	967	974	1078	1140
$\lambda_{\text{film onset}}$ (nm)	1090	1190	1304	1550
red shift (nm)	123	216	226	410
$E_g^{\text{opt.}}$ (eV)	1.14	1.04	0.95	0.80
E_g^{CV} (eV)[a]	1.36	1.26	1.21	0.75
$E_{\text{ox. onset}}$ (eV)	0.30	0.29	0.35	−0.05
$E_{\text{red. onset}}$ (eV)	−1.06	−0.92	−0.91	−0.80
VB (eV)[b]	−5.40	−5.39	−5.45	−5.05
CB (eV)[c]	−4.04	−4.18	−4.19	−4.30

[a] $E_g^{\text{opt.}} = 1240/\lambda_{\text{film onset}}$ eV. [b] VB = $-(5.10 + E_{\text{ox. onset}})$ eV. [c] CB = $-(5.10 + E_{\text{red. onset}})$ eV.

T2DEG show no distinct exothermal transitions in the second heating cycle, revealing the absence of significant degrees of crystallinity or phase transition across the measured temperature range (Figure S12, Supporting Information). For PNDI2OD-T2DO, the DSC curve shows a weak exotherm in the second heating cycle, indicative of a melting transition at 248 °C. However, PNDI2TEG-T2DEG shows three exotherms at 108, 209, and 274 °C in the second heating cycle and endotherms at 94, 191, and 253 °C in the first cooling cycle. These results indicate an increasingly complex thermal behavior commensurate with the inclusion of glycol ether chains, reflecting the general observation that pendant glycol ethers have a significant and complex influence on the morphology of π-conjugated materials and underscoring the need to investigate their influence in more depth.[33−42]

In order to gain insights into the effects of the side chains on the electronic structure, we carried out cyclic voltammetry (CV) on thin films of the polymers. The measurements were performed in acetonitrile under an inert atmosphere with 0.1 M *n*-Bu_4NPF_6, as the supporting electrolyte, a glassy carbon working electrode, a platinum wire counter electrode, and a Ag/AgCl pseudo-reference electrode. Ferrocene/ferrocenium (Fc/Fc^+) was used as an internal standard by assigning its half-wave potential an absolute energy of −5.1 eV *versus* vacuum.[43] The resulting plots from the first cycle (except PNDI2OD-T2DEG and PNDI2TEG-2DEG, for which the second reduction waves were selected) are shown in Figure 1, and the corresponding data are summarized in Table 1. All four copolymers show two quasi-reversible reduction and irreversible oxidation waves. The reduction waves are indicative of the NDI moiety in the polymer being reduced sequentially to form the NDI-polymer radical anion in the first reduction and then the NDI-polymer dianion in the second reduction. These reduction CV plots are similar to the classic n-type polymer P(NDI2OD-T2)[44−47] (Figure S14). The valence band (VB) and conductance band (CB) energy levels of these polymers are calculated from the onset of oxidation and reduction potentials using the equation $E_{VB} = -(5.10 + E_{\text{ox. onset}})$eV and $E_{CB} = -(5.10 + E_{\text{red. onset}})$ eV, respectively. The onset oxidation potentials of PNDI2OD-T2DO, PNDI2TEG-T2DO, PNDI2OD-T2DEG, and PNDI2TEG-T2DEG relative to Fc/Fc^+ were 0.30, 0.29, 0.35, and −0.05 V, respectively, which correspond to estimated VB energies of −5.40, −5.39, −5.45, and −5.05 eV. This trend suggests that the inclusion of glycol ethers has little effect except when installed on both monomers, in which case it destabilizes the VB by approximately 400 meV.

The onset of the reduction potentials of PNDI2OD-T2DO, PNDI2TEG-T2DO, PNDI2OD-T2DEG, and PNDI2TEG-T2DEG relative to Fc/Fc^+ are −1.06, −0.92, −0.91, and −0.80 V, respectively, which correspond to estimated CB energies of −4.04, −4.18, −4.19, and −4.30 eV. The relatively deep CB levels are the result of the strong electron affinity of the acceptor monomer (NDI) and indicate that all four copolymers have sufficient driving force for efficient charge transfer with an n-type dopant. The overall trend of the CB energies is PNDI2TEG-T2DEG < PNDI2TEG-T2DO = PNDI2OD-T2DEG < PNDI2OD-T2DO; these results clearly show that replacing pendant alkyl groups with glycol ethers systematically stabilizes the CB, suggesting that inductive effects have a significant effect on the electronic structure.

The glycol ether pendant groups may also tend to drive backbone crystallization, thus decreasing the difference in the torsional angle between bithiophene and adjacent NDI in the solid state compared to the solution, especially for PNDI2TEG-T2DEG, which is why the direct band transition is so much more red-shifted for the PNDI2TEG-T2DEG than for the others and why the VB (measured in thin films) shifts significantly compared to the highest occupied molecular orbital (measured in solution; see Figure S13 and density functional theory calculations in Supporting Information). Importantly, the CV data indicate that manipulating the pendant groups has a significant (inductive) effect on the electronic structure of the polymers that is distinct from and additive with morphological effects driven by the difference in polarity/polarizability of alkyl and glycol ether chains.

Figure 2 shows the UV−vis−NIR absorption spectra for pristine and doped D−A copolymer thin films. Films of PNDI2OD-T2DO, PNDI2TEG-T2DO, PNDI2OD-T2DEG, and PNDI2TEG-T2DEG show two characteristic absorption peaks of pristine polymers, which we assign to the $\pi-\pi^*$ transition (at around 400 nm) and the broad interband (charge-transfer) transition (P0, from 850 to 1000 nm).[18,28] We observed a relative bathochromic shift of the interband transitions for the copolymers bearing glycol ether groups relative to those bearing alkyl groups; the optical band gaps of PNDI2OD-T2DO, PNDI2TEG-T2DO, PNDI2OD-T2DEG, and PNDI2TEG-T2DEG determined from absorption onsets are 1.14, 1.04, 0.95, and 0.80 eV, respectively. The molecular doping of PNDI2OD-T2DO, PNDI2TEG-T2DO, and PNDI2OD-T2DEG causes a significant reduction in the absorptions associated with the pristine polymer and generates new polaron (P2′) absorptions at approximately 560 nm. The extent of this reduction can be affected by the doping level, the effective conjugation length, and the packing of conjugated polymers.[16] Thus, it is difficult to evaluate absolute doping levels among different D−A copolymers from the changes to the absorption spectra alone. The doping of PNDI2TEG-

https://doi.org/10.1021/acs.macromol.1c00317
Macromolecules 2021, 54, 3886−3896

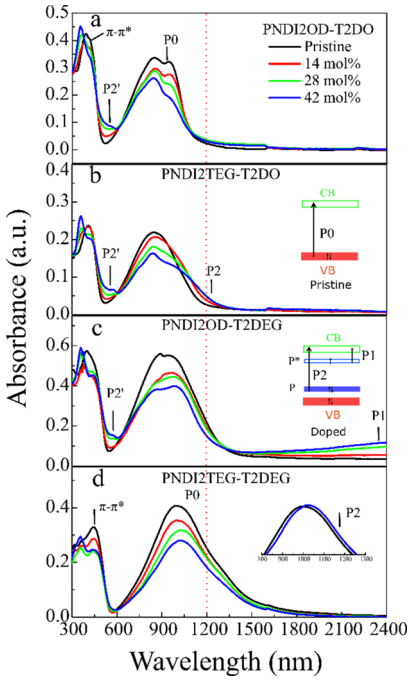

Figure 2. Ultraviolet−visible near infrared (UV−vis−NIR) absorption spectra of pristine and doped PNDI2OD-T2DO, PNDI2TEG-T2DO, PNDI2OD-T2DEG, and PNDI2TEG-T2DEG films.

T2DO gives rise to a bathochromic shift in the low-energy absorption onset, which we ascribe to the overlap of neutral CT absorption and polaron transition (P2) absorption. However, we did not see the polaron absorption peak (P1) in the doping of PNDI2TEG-T2DO, which might be due to the mixing of the newly formed polaron band with the CB. The low-energy absorption at $\lambda > 1500$ nm that appears in doped PNDI2OD-T2DEG is either a subgap, P1 polaron absorption, scattering (see the discussion of film morphology below) or both; a (P1) peak at around 3000 nm (0.41 eV) grows with dopant concentration, indicating a commensurate increase in the doping level (see full spectra in Figure S17). Thermodynamically, PNDI2TEG-T2DEG is most prone to be doped by *n*-DMBI as it exhibits the lowest CB energy among the four D−A copolymers. However, the molecular doping of PNDI2TEG-T2DEG only causes a reduction in the pristine absorbances, without a commensurate rise in P1 and P2 absorbances. Normalizing the absorption spectra of pristine PNDI2TEG-T2DEG films reveals a bathochromic shift in the P0 (pristine inter-band) absorbance with increasing dopant concentration, which may be indicative of a P2 transition. Polaron bands formed by molecular doping tend to have an energy level lower than the CB or higher than the VB due to the reorganization energy of the backbones responding to a change in the oxidation state.[48] Thus, polaron features P2 and P1 are visible in the absorption spectra. For PNDI2TEG-T2DEG, the glycol ether pendant groups may reduce the reorganization energy, improving the electronic overlap in the pristine state, which is evident in the broader absorption between 600 and 1550 nm. In this scenario, the polaron bands would be too close in energy to the VBs/CBs to produce discrete absorption peaks. The results of UV−vis−NIR absorption spectra confirm that the D−A copolymers are doped by *n*-DMBI, but they do not provide further insights into the absolute doping efficiencies.

In order to characterize and compare the thermoelectric properties of these four copolymers, we checked the electrical conductivity and the Seebeck coefficient of the doped conjugated copolymers. The doped thin films were prepared from mixtures of copolymer and *n*-DMBI in varied molar fractions in a nitrogen-filled glovebox by spin coating on glass substrates on which parallel line-shaped gold electrodes were previously deposited as the bottom contacts, which were then

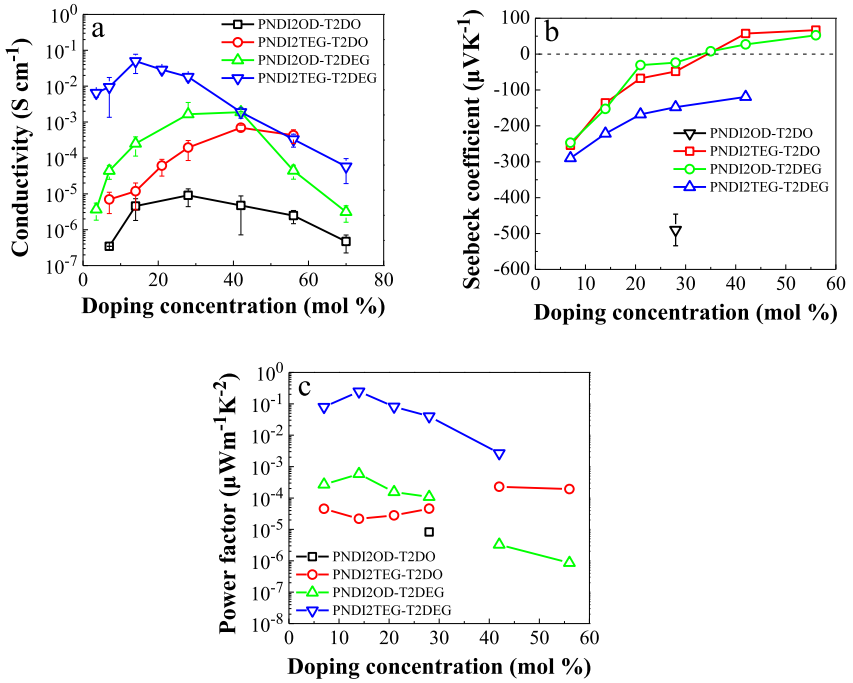

Figure 3. (a) Electrical conductivities, (b) Seebeck coefficients, and (c) PF of doped PNDI2OD-T2DO, PNDI2TEG-T2DO, PNDI2OD-T2DEG, and PNDI2TEG-T2DEG thin films.

https://doi.org/10.1021/acs.macromol.1c00317
Macromolecules 2021, 54, 3886−3896

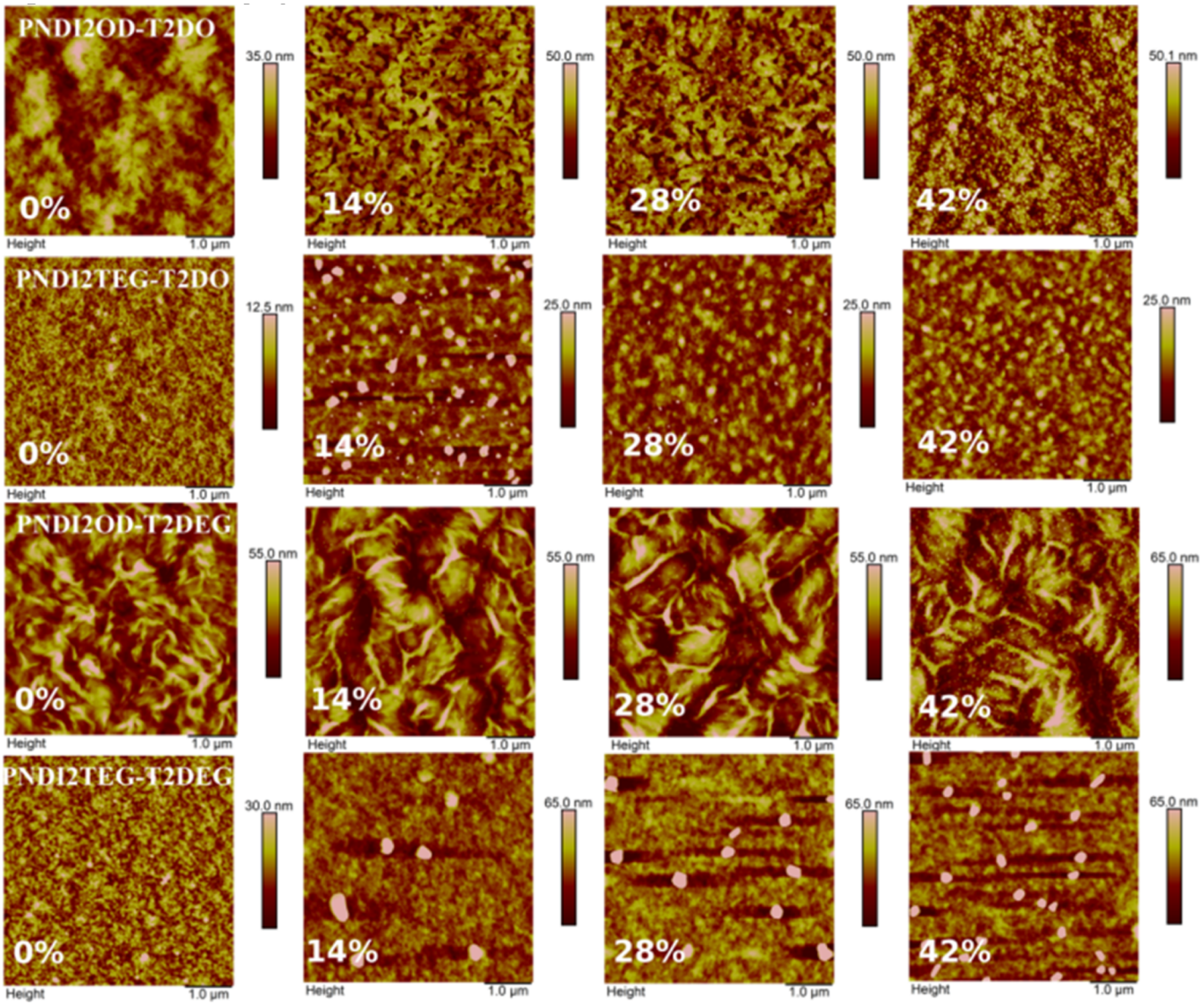

Figure 4. AFM images of pristine and doped PNDI2OD-T2DO, PNDI2TEG-T2DO, PNDI2OD-T2DEG, and PNDI2TEG-T2DEG thin films in a pristine state (0 mol %) and at various doping concentrations (14, 28, 42 mol %).

subjected to thermal annealing at 120 °C for 1 h Figure 3a shows the electrical conductivities (σ) of the four doped D−A copolymers at different doping concentrations. Among the four doped D−A copolymers, doped PNDI2OD-T2DO (which has alkyl groups on both monomers) shows the lowest electrical conductivity with an optimized value of $9.1 \pm 4.7 \times 10^{-6}$ S cm^{-1} at a doping concentration of 28 mol %. Replacing any one of the alkyl side chains with a glycol ether side chain leads to an increase in electrical conductivity; PNDI2TEG-T2DO and PNDI2OD-T2DEG give optimized electrical conductivities of $7.0 \pm 1.2 \times 10^{-4}$ and $1.9 \pm 0.1 \times 10^{-3}$ S cm^{-1}, respectively, at a doping concentration of 42 mol %. Doped PNDI2TEG-T2DEG (which has glycol ether chains on both monomers) shows the highest electrical conductivity of all four copolymers, giving a value of $5.0 \pm 2.7 \times 10^{-2}$ S cm^{-1} at a doping concentration of 14 mol %. In all cases, the substitution of an alkyl chain by a glycol ether increases the conductivity. These results indicate that the side chains play an important role in the n-doping of D−A copolymers, presumably by affecting not only the packing of the polymer chains but also their interactions with dopant molecules.

S is determined by the difference in energy between the Fermi level (E_F) and the charge-transport level (E_T).[49] Typically, as more charges are generated *via* molecular doping, E_F shifts toward E_T and the absolute value of S decreases. Figure 3b shows the values of S for the doped D−A copolymers. The resistance of films of lightly doped PNDI2OD-T2DO was too large to measure thermal voltages accurately; thus values of $S = -490 \pm 44$ μV K^{-1} could only be determined for 28 mol %-doped films. For films of PNDI2TEG-T2DEG, $S = -289.8$ μV K^{-1} at a doping concentration of 7 mol %. The negative sign indicates that the dominant charge carriers are electrons. At a doping concentration of 42 mol %, S decreases to -119.1 μV K^{-1}, reflecting the decreasing gap between E_F and E_T as the doping level increases; that is, the level of doping increases with the concentration of the dopant. At a doping concentration of 7 mol %, films of PNDI2TEG-T2DO and PNDI2OD-T2DEG show similar values of S of -254.5 ± 2.5 and -247 ± 8.6 μV K^{-1}, respectively, which are comparable to the doped films of PNDI2TEG-T2DEG. The similarity in the magnitude of S suggests similar doping levels for the films of PNDI2TEG-

https://doi.org/10.1021/acs.macromol.1c00317
Macromolecules 2021, 54, 3886−3896

T2DO, PNDI2OD-T2DEG, and PNDI2TEG-T2DEG at a doping concentration of 7 mol %; that is, the copolymers bifurcate into two groups, those bearing only alkyl chains and those bearing any number of glycol ether chains. As the doping concentration increases from 7 to 28 mol %, the absolute values of S for the films of PNDI2OD-T2DO and PNDI2OD-T2DEG decrease, as expected; however, increasing the doping concentration from 28 to 56 mol % results in the unusual observation of the sign of S switching (from negative to positive), crossing zero near 35 mol %. Interestingly, S goes to zero at the peak of the electrical conductivity (see Figure 3a). Sign switching of S has been reported for the electrochemical doping of poly(ethylenedioxythiophene):poly-(styrenesulphonate) (PEDOT:PSS) and the chemical doping of poly(pyridinium phenylene) [P(PymPh)] with a strong reducing agent;[49,50] however, in those cases, the polymers are much more heavily doped than in this work. For both PEDOT:PSS and P(PymPh), the interband absorption of the pristine polymer is lost completely at the point of sign switching, leading to electrical conductivities of more than 10 S cm^{-1}. The molecular doping process in our work is comparatively weaker, as is evident by the slight reduction in the pristine absorption (Figure 2) and lower electrical conductivities of $\sim 10^{-3}$ S cm^{-1}. As such, the mechanism for the sign switching of S in the D−A copolymers is different from those reported in previous studies. We hypothesize that it is because charge transport occurs through doping-induced gap states, which form below E_F and, therefore, have a contribution to S that is positive in sign irrespective of the sign of the carriers, similar to the behavior that we have observed in other molecularly doped polymer films.[51]

Based on the aforementioned electrical conductivities and Seebeck coefficients, we calculated the PFs of the doped films, which are summarized in Figure 3c. Films of PNDI2OD-T2DO at a doping concentration of 14 mol % showed a relatively small PF of 8.6×10^{-6} μW m^{-1} K^{-2} due to its low conductivity. Films of PNDI2TEG-T2DO and PNDI2OD-T2DEG exhibited slightly high PF on the order of 10^{-5} μW m^{-1} K^{-2} before the sign switching of S. In contrast, films of PNDI2TEG-T2DEG gave the highest PF, 0.24 μW m^{-1} K^{-2}. Our results unambiguously indicate that the n-type thermoelectric performance scales with the inclusion of glycol ether side chains.

Previous studies have highlighted the importance of the solubility of the dopant in the host polymer in n-type molecular doping.[10,52] In order to gain insights into this solubility for our D−A copolymer systems, we characterized the topography of the pristine and doped films by AFM, the results of which are shown in Figure 4. Pristine films of PNDI2OD-T2DO and PNDI2TEG-T2DEG (which have matching pendant groups on the monomers) show relatively smooth surfaces with root mean square roughnesses of 5.7 and 4.8 nm, respectively, compared to 2 nm for pristine PNDI2TEG-T2DO and 10.1 nm for pristine PNDI2OD-T2DEG (which have mismatched pendant groups). Many factors contribute to the final film morphology, but the mismatch in polarity/polarizability apparently drives a self-assembly process[53] in PNDI2OD-T2DEG that is not present in PNDI2TEG-T2DO (where the positions of the pendant groups are swapped) and that leads to the petal-shaped nanostructures, as shown in Figure 4. While the topology of the films of PNDI2OD-T2DO evolved significantly with increasing doping concentration, films of PNDI2TEG-T2DO, PNDI2OD-T2DEG, and PNDI2TEG-T2DEG showed no obvious change. Small, ovaloid recessions (shown in black) also appeared on the surface of doped PNDI2OD-T2DO with increasing density as more dopant was added. We ascribe the changing topography to the formation of aggregates, likely caused by the relatively poor solubility of the dopant in the matrix of the D−A copolymer, driving phase segregation between the polar/charged dopant and the apolar pendant groups. Replacing the alkyl chains with polar glycol ether chains has a stark influence on the evolution of the topography. For example, the topography of the doped PNDI2OD-T2DEG (which has polar chains on the D monomer) changes very little with doping. In the films of PNDI2TEG-T2DEG (which has polar chains on both monomers), the topography remains mostly homogenous, even at a doping concentration of 42 mol %. We hypothesize that the inclusion of polar chains favors the formation of charge-transfer species rather than aggregates of pure dopant phase separating from the polymer.

Although the pendant groups have a substantial influence on the topography, we can only speculate as to what the various features comprise. Thus, to gain further insights into phase segregation and dispersal of the dopant in the films, we acquired spatially resolved absorption spectroscopy (SRAS) images of the 42 mol %-doped films. The spatial resolution is around 500 nm (optical resolution limit), resulting in hyperspectral 40 × 40 μm images with 6640 pixels and each pixel corresponding to a full absorption spectrum (experimental details in Supporting Information). For each sample, we show the averaged absorption spectrum, normalized to the absorbance at 850 nm, as a thick blue line in Figure 5a−d. Those averaged spectra closely reproduce the corresponding ensemble spectra given in Figure 2, with the deviations at 900−1000 nm likely being related to the substantial drop in detection efficiency in this spectral range.

For a more detailed analysis, we retrieve from each individual spectrum in the hyperspectral data sets the ratio A_{600}/A_{850} of absorbances at 600 and 850 nm. Based on Figure 2, this ratio serves as a relative measure for the doping level, and it increases upon doping. The blue shaded areas in Figure 5a−d represent the variation in A_{600}/A_{850} that was found on each sample. The upper (lower) limit of this area was constructed by averaging the percentile of spectra that showed the highest (lowest) ratio A_{600}/A_{850}. We found that the spectral variation is largest for PNDI2OD-T2DEG (Figure 5c), intermediate for PNDI2TEG-T2DO (Figure 5b), and small for PNDI2OD-T2OD and PNDI2TEG-T2DEG (Figure 5a,d). Given that this ratio is a measure for the relative doping efficiency, these data indicate that on length scales of the optical resolution, there are significant local variations in doping efficiency for PNDI2OD-T2DEG. For PNDI2TEG-T2DO, PNDI2OD-T2OD, and PNDI2TEG-T2DEG, these local variations are less pronounced. That is, the less pronounced those spectral variations, the more evenly distributed the doping levels and, by extension, the dopant are. We note that the spectral variation in pristine (undoped) PNDI2TOD-T2DEG films is relatively small due to the absence of the dopant (Figure S20).

The spatial variation of the doping level is visualized in Figure 5e−h, which displays 20 × 20 μm heat maps of the ratio A_{650}/A_{850}. For PNDI2OD-T2DEG, we detect variations on the length scale of several μm, while for PNDITEG-T2DO and particularly for PNDI2OD-T2OD and PNDI2TED-T2DEG, those variations are increasingly less visible. These observations

https://doi.org/10.1021/acs.macromol.1c00317
Macromolecules 2021, 54, 3886−3896

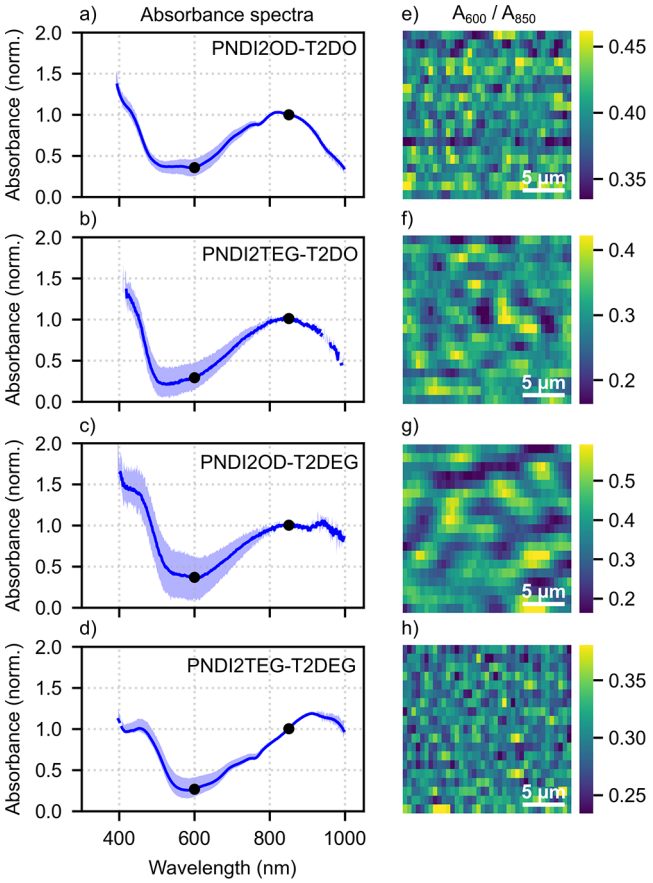

Figure 5. Spatially resolved absorption spectra on 42 mol % doped copolymer films. (a–d) Average spectra (thick blue line) and spectral variations (blue shaded area); for details, see text. (e–h) 20 × 20 μm maps of the absorption ratio A_{600}/A_{850}.

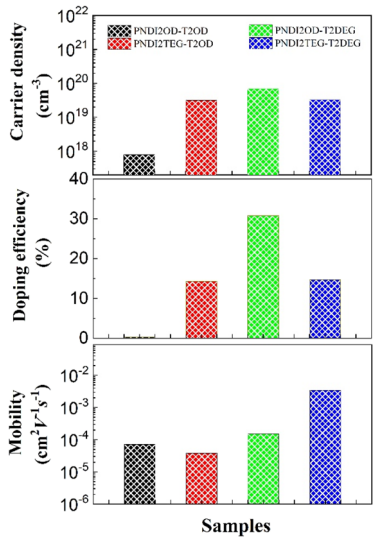

Figure 6. Carrier density (top panel), doping efficiency (middle panel), and mobility (bottom panel) of 28 mol %-doped PNDI2OD-T2DO, PNDI2TEG-T2DO, PNDI2OD-T2DEG, and PNDI2TEG-T2DEG thin films.

nicely agree with feature sizes in the AFM images (Figure 4). Thus, we believe that the spatial variation of doping levels is directly linked to the presence of large aggregates, with doping levels depending not only on the chemical structure of the copolymer but also on its local molecular packing, which is highly sensitive to the regiochemistry of the pendant groups.

From the AFM and SRAS data, we conclude that the polar pendant groups promote the dissolution of the polar/ionized dopant in the polymer matrix, although with sometimes significant spatial variation, and that the regiochemistry of the chains has a significant impact on the organization and self-assembly of the pristine and doped films.

In our previous work, we measured the carrier density (n) of films of doped organic semiconductors directly by using admittance spectroscopy on a metal–insulator–semiconductor device with an ion gel insulating layer (PVDF-HFP:[EMIM]-[TFSI] blend).[27] The composition of the ion gel was carefully optimized to achieve a capacitance of around 3 μF cm^{-2} and sufficient mechanical robustness to withstand the sequential coating of the active layer. The capacitance *versus* DC voltage plot of the four doped D–A copolymers (28 mol %) is shown in Figure S18. Based on the Mott–Schottky analysis (see the experimental methods), the carrier densities in the four 28%-doped D–A copolymers were extracted (the top panel of Figure 6). The doped PNDI2OD-T2DO yielded a carrier density of 7.9 × 10^{17} cm^{-3}, the lowest of the series. In contrast, films of doped PNDI2TEG-T2DO, PNDI2OD-T2DEG, and PNDI2TEG-T2DEG exhibited much higher carrier densities of 3.2 × 10^{19}, 6.9 × 10^{19}, and 3.3 × 10^{19} cm^{-3}, respectively, translating to respective doping efficiencies of 14, 31, and 14% (assuming the total site density of N = 8 × 10^{20} cm^{-3}). These densities are more than 40 times greater than for PNDI2OD-T2DO, further confirming the effectiveness of glycol ether chains in molecular n-doping of D–A copolymers. Here again, however, regiochemistry and not just the presence or absence of glycol ether chains matters; films of PNDI2OD-T2DEG gave 31% doping efficiency, which is double that of PNDI2TEG-T2DEG.

This observation cannot be explained by a simple relationship between the number or volume fraction of polar(izable) chains and the host/dopant miscibility, as PNDI2OD-T2DEG has one fewer glycol ether chain than PNDI2TEG-T2DEG. Rather, we hypothesize that the unusual morphology observed by AFM is the result of the specific regiochemistry and is a manifestation of self-assembly at the polymer dopant scale. It is well established that, by design, the unoccupied molecular orbitals of D–A copolymer tend to be localized on the acceptor monomer, which in this case is an NDI moiety.[54] The glycol ether chains of PNDI2OD-T2DEG are attached to the electron-rich (donor) bithiophene moiety. It is, therefore, reasonable to assume that the ionized dopant molecules would be, on average, closer to bithiophene than to the NDI moiety both because of the cationic nature of the dopant and the highly polar glycol ether chains; that is, if the polymer chains pack to create lipophilic domains of alkyl groups, dopant molecules will prefer the commensurate glycol ether phase. Recently, we reported that glycol ether pendant groups effectively control how dopant molecules incorporate into a host conjugated polymer matrix, leading to a negligible effect on the π–π packing but increased doping efficiency and PF.[27,55] Salzmann *et al.* suggested a way to increase doping efficiency by sterically blocking the dopant from interacting with unoccupied molecular orbitals, thus preventing strong electronic overlap (or localized charge-transfer).[3] We postulate that the disparate polarities of the pendant groups accomplish exactly that, by providing a thermodynamic driving force to

https://doi.org/10.1021/acs.macromol.1c00317
Macromolecules 2021, 54, 3886–3896

associate with the bithiophene rather than the NDI, thus causing an improved doping efficiency in the doped PNDI2OD-T2DEG, though with significant spatial variations (Figure 5c,g) driven by the self-assembly of the polymer chains. This driving force would likely require sufficient ordering in the solid state to create disparate hydrophobic and hydrophilic microenvironments *via* interpolymer interactions. Such ordering is plausible, given the rigidity and tendency of NDI to π-stack, the bulk of the branched alkyl chains, the preference for bithiophene to adopt an anticonfiguration, and the pronounced impact glycol ether chains have on morphology.[19,30,35,36,43,45] The optical spectra (Figure 2c and some extent Figure 5c) further support this hypothesis, exhibiting strong evidence of π-stacking of the NDI due to the shape of the $\pi-\pi^*$ transition, which changes quite strongly in a characteristic way. While direct evidence of such ordering is not possible, the AFM images reveal a substantially different topography on a very different length scale in the films of PNDI2OD-T2DEG as compared to the other D−A copolymers, which is a strong indication of different packing.

Based on the measured values of electrical conductivity and carrier density, the bulk mobility values of films of the D−A copolymers were 7.2×10^{-5}, 3.8×10^{-5}, 1.5×10^{-4}, and 3.5×10^{-3} cm^2 (V s)$^{-1}$, respectively. The trend diverges from previous observations that glycol ether side chains cause mobilities to decrease;[27,28] PNDI2TEG-T2DEG has both the highest mobility and the highest fraction of glycol ethers. This observation suggests that functionalization of the bithiophene units counteracts any negative impacts that glycol ethers might otherwise have on the ability of the polymer chains to pack and further underscores the importance of not just the identity but also the regiochemistry of side chains in molecularly doped films of conjugated polymers.

CONCLUSIONS

The design rules for conjugated polymers that operate while doped must cope with the added complexity that the incorporation of dopants brings. Particularly for n-type polymers, which must be dopable by reducing agents that are sufficiently (air) stable to process. We investigated the influence of the identity and regiochemistry of side chains on molecular doping with *n*-DMBI by synthesizing and characterizing four different combinations of polar(izable), glycol ether, and alkyl pendant groups on an NDI-bithiophene D−A copolymer backbone and measuring their properties at different doping levels. Surprisingly, despite being attached *via* ether linkages, the primary electronic effect of the addition of glycol ether was to increase electron affinity while, at the same time, increasing the solubility of (ionized) *n*-DMBI dopant molecules in the film, leading to a factor of 40 increase in doping efficiency and an optimized conductivity of 0.08 S cm^{-1} in the polymer with all glycol ether pendant groups. Surprisingly, maximum doping efficiency was not commensurate with the increased volume fraction of glycol ether chains. Rather, the combination of the identity and regiochemistry of the side chains produced the highest carrier density and doping efficiency. Spatially resolved absorption spectra revealed a correlation between doping efficiency and AFM topology, from which we concluded that the combination of alkyl chains on the acceptor and glycol ether chains on the donor drive the dopant molecules to associate with the donor, minimizing the unwanted electronic overlap between the dopant and unoccupied molecular orbitals. While a further study on the wider scope of backbones and pendant groups is needed to develop consistent design rules, particularly with respect to self-assembly driving large morphological changes, this work highlights an important design principle that must be taken into account for the future design of conjugated polymers optimized for molecular doping.

ASSOCIATED CONTENT

Supporting Information

The Supporting Information is available free of charge at https://pubs.acs.org/doi/10.1021/acs.macromol.1c00317.

Detailed description of the synthesis and characterization of the materials; NMR and IR spectra; GPC curves; TGA and DSC curves; UV−vis−NIR spectra; DFT calculation; CP-AFM images and device fabrication and measurement; and spatially resolved absorption measurement and other data (PDF)

AUTHOR INFORMATION

Corresponding Authors

Jian Liu − *Zernike Institute for Advanced Materials, NL-9747 AG Groningen, The Netherlands;* orcid.org/0000-0002-6704-3895; Email: Jian.liu@rug.nl

L. Jan Anton Koster − *Zernike Institute for Advanced Materials, NL-9747 AG Groningen, The Netherlands;* orcid.org/0000-0002-6558-5295; Email: l.j.a.koster@rug.nl

Ryan C. Chiechi − *Stratingh Institute for Chemistry, NL-9747 AG Groningen, The Netherlands; Zernike Institute for Advanced Materials, NL-9747 AG Groningen, The Netherlands;* orcid.org/0000-0002-0895-2095; Email: r.c.chiechi@rug.nl

Authors

Gang Ye − *Center for Biomedical Optics and Photonics (CBOP) & College of Physics and Optoelectronic Engineering, Key Laboratory of Optoelectronic Devices and Systems, Shenzhen University, Shenzhen 518060, P. R. China; Stratingh Institute for Chemistry, NL-9747 AG Groningen, The Netherlands; Zernike Institute for Advanced Materials, NL-9747 AG Groningen, The Netherlands*

Xinkai Qiu − *Stratingh Institute for Chemistry, NL-9747 AG Groningen, The Netherlands; Zernike Institute for Advanced Materials, NL-9747 AG Groningen, The Netherlands*

Sebastian Stäter − *Zernike Institute for Advanced Materials, NL-9747 AG Groningen, The Netherlands*

Li Qiu − *Yunnan Key Laboratory for Micro/Nano Materials & Technology, National Center for International Research on Photoelectric and Energy Materials, School of Materials and Energy, Yunnan University, Kunming 650091, P. R. China;* orcid.org/0000-0001-5838-0593

Yuru Liu − *Stratingh Institute for Chemistry, NL-9747 AG Groningen, The Netherlands; Zernike Institute for Advanced Materials, NL-9747 AG Groningen, The Netherlands*

Xuwen Yang − *Zernike Institute for Advanced Materials, NL-9747 AG Groningen, The Netherlands*

Richard Hildner − *Zernike Institute for Advanced Materials, NL-9747 AG Groningen, The Netherlands;* orcid.org/0000-0002-7282-3730

Complete contact information is available at: https://pubs.acs.org/10.1021/acs.macromol.1c00317

https://doi.org/10.1021/acs.macromol.1c00317
Macromolecules 2021, 54, 3886−3896

Notes

The authors declare no competing financial interest.

■ ACKNOWLEDGMENTS

This work was supported by a grant from STW/NWO (VIDI 13476). This work is part of the research program of the Foundation of Fundamental Research on Matter (FOM), which is part of the Netherlands Organization for Scientific Research (NWO). This is a publication by the FOM Focus Group "Next Generation Organic Photovoltaics", participating in the Dutch Institute for Fundamental Energy Research (DIFFER). G.Y. acknowledges the China Postdoctoral Science Foundation Funded Project (grant 2020M672771) and Guangdong Basic and Applied Basic Research Foundation (2020A1515110636). Y.L. and X.Y. acknowledge financial support from the China Scholarship Council (CSC). L.Q. acknowledges the National Natural Science Foundation of China (51962036). We would like to greatly thank Dr. Jianhua Chen and Prof. Dr. Xugang Guo from South University of Science and Technology of China (SUSTC) for GPC measurement.

■ REFERENCES

(1) Jacobs, I. E.; Moulé, A. J. Controlling Molecular Doping in Organic Semiconductors. *Adv. Mater.* **2017**, *29*, 1703063.
(2) Zhang, Y.; Zhou, H.; Seifter, J.; Ying, L.; Mikhailovsky, A.; Heeger, A. J.; Bazan, G. C.; Nguyen, T.-Q. Molecular Doping Enhances Photoconductivity in Polymer Bulk Heterojunction Solar Cells. *Adv. Mater.* **2013**, *25*, 7038−7044.
(3) Salzmann, I.; Heimel, G.; Oehzelt, M.; Winkler, S.; Koch, N. Molecular Electrical Doping of Organic Semiconductors: Fundamental Mechanisms and Emerging Dopant Design Rules. *Acc. Chem. Res.* **2016**, *49*, 370−378.
(4) Kolesov, V. A.; Fuentes-Hernandez, C.; Chou, W.-F.; Aizawa, N.; Larrain, F. A.; Wang, M.; Perrotta, A.; Choi, S.; Graham, S.; Bazan, G. C.; et al. Solution-Based Electrical Doping of Semiconducting Polymer Films over a Limited Depth. *Nat. Mater.* **2017**, *16*, 474−480.
(5) Lüssem, B.; Riede, M.; Leo, K. Doping of Organic Semiconductors. *Phys. Status Solidi* **2013**, *210*, 9−43.
(6) Günther, A. A.; Sawatzki, M.; Formánek, P.; Kasemann, D.; Leo, K. Contact Doping for Vertical Organic Field-Effect Transistors. *Adv. Funct. Mater.* **2016**, *26*, 768−775.
(7) Lu, G.; Blakesley, J.; Himmelberger, S.; Pingel, P.; Frisch, J.; Lieberwirth, I.; Salzmann, I.; Oehzelt, M.; Di Pietro, R.; Salleo, A.; et al. Moderate Doping Leads to High Performance of Semiconductor/Insulator Polymer Blend Transistors. *Nat. Commun.* **2013**, *4*, 1588.
(8) Kim, G.-H.; Shao, L.; Zhang, K.; Pipe, K. P. Engineered Doping of Organic Semiconductors for Enhanced Thermoelectric Efficiency. *Nat. Mater.* **2013**, *12*, 719−723.
(9) Glaudell, A. M.; Cochran, J. E.; Patel, S. N.; Chabinyc, M. L. Impact of the Doping Method on Conductivity and Thermopower in Semiconducting Polythiophenes. *Adv. Energy Mater.* **2015**, *5*, 1401072.
(10) Schlitz, R. A.; Brunetti, F. G.; Glaudell, A. M.; Miller, P. L.; Brady, M. A.; Takacs, C. J.; Hawker, C. J.; Chabinyc, M. L. Solubility-Limited Extrinsic n-Type Doping of a High Electron Mobility Polymer for Thermoelectric Applications. *Adv. Mater.* **2014**, *26*, 2825−2830.
(11) Karpov, Y.; Erdmann, T.; Raguzin, I.; Al-Hussein, M.; Binner, M.; Lappan, U.; Stamm, M.; Gerasimov, K. L.; Beryozkina, T.; Bakulev, V.; et al. High Conductivity in Molecularly P-Doped Diketopyrrolopyrrole-Based Polymer: The Impact of a High Dopant Strength and Good Structural Order. *Adv. Mater.* **2016**, *28*, 6003−6010.
(12) Kroon, R.; Kiefer, D.; Stegerer, D.; Yu, L.; Sommer, M.; Müller, C. Polar Side Chains Enhance Processability, Electrical Conductivity, and Thermal Stability of a Molecularly p-Doped Polythiophene. *Adv. Mater.* **2017**, *29*, 1700930.
(13) Patel, S. N.; Glaudell, A. M.; Peterson, K. A.; Thomas, E. M.; O'Hara, K. A.; Lim, E.; Chabinyc, M. L. Morphology Controls the Thermoelectric Power Factor of a Doped Semiconducting Polymer. *Sci. Adv.* **2017**, *3*, No. e1700434.
(14) Jacobs, I. E.; Aasen, E. W.; Oliveira, J. L.; Fonseca, T. N.; Roehling, J. D.; Li, J.; Zhang, G.; Augustine, M. P.; Mascal, M.; Moulé, A. J. Comparison of Solution-Mixed and Sequentially Processed P3HT:F4TCNQ FFlms: Effect of Doping-Induced Aggregation on Film Morphology. *J. Mater. Chem. C* **2016**, *4*, 3454−3466.
(15) Müller, L.; Nanova, D.; Glaser, T.; Beck, S.; Pucci, A.; Kast, A. K.; Schröder, R. R.; Mankel, E.; Pingel, P.; Neher, D.; et al. Charge-Transfer-Solvent Interaction Predefines Doping Efficiency in p-Doped P3HT Films. *Chem. Mater.* **2016**, *28*, 4432−4439.
(16) Naab, B. D.; Gu, X.; Kurosawa, T.; To, J. W. F.; Salleo, A.; Bao, Z. Role of Polymer Structure on the Conductivity of N-Doped Polymers. *Adv. Electron. Mater.* **2016**, *2*, 1600004.
(17) Shi, K.; Zhang, F.; Di, C.-A.; Yan, T.-W.; Zou, Y.; Zhou, X.; Zhu, D.; Wang, J.-Y.; Pei, J. Toward High Performance N-Type Thermoelectric Materials by Rational Modification of BDPPV Backbones. *J. Am. Chem. Soc.* **2015**, *137*, 6979−6982.
(18) Wang, S.; Sun, H.; Ail, U.; Vagin, M.; Persson, P. O. Å.; Andreasen, J. W.; Thiel, W.; Berggren, M.; Crispin, X.; Fazzi, D.; et al. Thermoelectric Properties of Solution-Processed n-Doped Ladder-Type Conducting Polymers. *Adv. Mater.* **2016**, *28*, 10764−10771.
(19) Liu, J.; Ye, G.; van der Zee, B.; Dong, J.; Qiu, X.; Liu, Y.; Portale, G.; Chiechi, R. C.; Koster, L. J. A. N-Type Organic Thermoelectrics of Donor-Acceptor Copolymers: Improved Power Factor by Molecular Tailoring of the Density of States. *Adv. Mater.* **2018**, *30*, 1804290.
(20) Wang, S.; Sun, H.; Erdmann, T.; Wang, G.; Fazzi, D.; Lappan, U.; Puttisong, Y.; Chen, Z.; Berggren, M.; Crispin, X.; et al. A Chemically Doped Naphthalenediimide-Bithiazole Polymer for n-Type Organic Thermoelectrics. *Adv. Mater.* **2018**, *30*, 1801898.
(21) Yang, C.-Y.; Jin, W.-L.; Wang, J.; Ding, Y.-F.; Nong, S.; Shi, K.; Lu, Y.; Dai, Y.-Z.; Zhuang, F.-D.; Lei, T.; et al. Enhancing the N-Type Conductivity and Thermoelectric Performance of Donor-Acceptor Copolymers through Donor Engineering. *Adv. Mater.* **2018**, *30*, 1802850.
(22) Yan, X.; Xiong, M.; Li, J.-T.; Zhang, S.; Ahmad, Z.; Lu, Y.; Wang, Z.-Y.; Yao, Z.-F.; Wang, J.-Y.; Gu, X.; Lei, T. Pyrazine-Flanked Diketopyrrolopyrrole (DPP): A New Polymer Building Block for High-Performance n-Type Organic Thermoelectrics. *J. Am. Chem. Soc.* **2019**, *141*, 20215−20221.
(23) Wang, Y.; Takimiya, K. Naphthodithiophenediimide-Bithiopheneimide Copolymers for High-Performance n-Type Organic Thermoelectrics: Significant Impact of Backbone Orientation on Conductivity and Thermoelectric Performance. *Adv. Mater.* **2020**, *32*, 2002060.
(24) Zhang, X.; Richter, L. J.; Delongchamp, D. M.; Kline, R. J.; Hammond, M. R.; McCulloch, I.; Heeney, M.; Ashraf, R. S.; Smith, J. N.; Anthopoulos, T. D.; et al. Molecular Packing of High-Mobility Diketo Pyrrolo-Pyrrole Polymer Semiconductors with Branched Alkyl Side Chains. *J. Am. Chem. Soc.* **2011**, *133*, 15073−15084.
(25) Himmelberger, S.; Duong, D. T.; Northrup, J. E.; Rivnay, J.; Koch, F. P. V.; Beckingham, B. S.; Stingelin, N.; Segalman, R. A.; Mannsfeld, S. C. B.; Salleo, A. Role of Side-Chain Branching on Thin-Film Structure and Electronic Properties of Polythiophenes. *Adv. Funct. Mater.* **2015**, *25*, 2616−2624.
(26) Zhao, W.; Ding, J.; Zou, Y.; Di, C.-a.; Zhu, D. Chemical Doping of Organic Semiconductors for Thermoelectric Applications. *Chem. Soc. Rev.* **2020**, *49*, 7210−7228.
(27) Liu, J.; Qiu, L.; Alessandri, R.; Qiu, X.; Portale, G.; Dong, J. J.; Talsma, W.; Ye, G.; Sengrian, A. A.; Souza, P. C. T.; et al. Enhancing Molecular N-Type Doping of Donor−Acceptor Copolymers by Tailoring Side Chains. *Adv. Mater.* **2018**, *30*, 1704630.

https://doi.org/10.1021/acs.macromol.1c00317
Macromolecules 2021, 54, 3886−3896

(28) Giovannitti, A.; Nielsen, C. B.; Sbircea, D.-T.; Inal, S.; Donahue, M.; Niazi, M. R.; Hanifi, D. A.; Amassian, A.; Malliaras, G. G.; Rivnay, J.; et al. Erratum: N-Type Organic Electrochemical Transistors with Stability in Water. *Nat. Commun.* **2016**, *7*, 13066.
(29) Kiefer, D.; Giovannitti, A.; Sun, H.; Biskup, T.; Hofmann, A.; Koopmans, M.; Cendra, C.; Weber, S.; Anton Koster, L. J.; Olsson, E.; Müller, C.; et al. Enhanced N-Doping Efficiency of a Naphthalenediimide-Based Copolymer through Polar Side Chains for Organic Thermoelectrics. *ACS Energy Lett.* **2018**, *3*, 278−285.
(30) Higginbotham, H. F.; Maniam, S.; Langford, S. J.; Bell, T. D. M. New Brightly Coloured, Water Soluble, Core-Substituted Naphthalene Diimides for Biophysical Applications. *Dyes Pigm.* **2015**, *112*, 290−297.
(31) Guo, X.; Watson, M. D. Conjugated Polymers from Naphthalene Bisimide. *Org. Lett.* **2008**, *10*, 5333−5336.
(32) Zhao, H.; Zhu, B.; Sekine, J.; Luo, S.-C.; Yu, H.-h. Oligoethylene-Glycol-Functionalized Polyoxythiophenes for Cell Engineering: Syntheses, Characterizations, and Cell Compatibilities. *ACS Appl. Mater. Interfaces* **2012**, *4*, 680−686.
(33) Song, C. K.; Eckstein, B. J.; Tam, T. L. D.; Trahey, L.; Marks, T. J. Conjugated Polymer Energy Level Shifts in Lithium-Ion Battery Electrolytes. *ACS Appl. Mater. Interfaces* **2014**, *6*, 19347−19354.
(34) Kanimozhi, C.; Yaacobi-Gross, N.; Chou, K. W.; Amassian, A.; Anthopoulos, T. D.; Patil, S. Diketopyrrolopyrrole-Diketopyrrolopyrrole-Based Conjugated Copolymer for High-Mobility Organic Field-Effect Transistors. *J. Am. Chem. Soc.* **2012**, *134*, 16532−16535.
(35) Chen, X.; Zhang, Z.; Liu, J.; Wang, L. A Polymer Electron Donor Based on Isoindigo Units Bearing Branched Oligo(Ethylene Glycol) Side Chains for Polymer Solar Cells. *Polym. Chem.* **2017**, *8*, 5496−5503.
(36) Chen, X.; Zhang, Z.; Ding, Z.; Liu, J.; Wang, L. Diketopyrrolopyrrole-Based Conjugated Polymers Bearing Branched Oligo(Ethylene Glycol) Side Chains for Photovoltaic Devices. *Angew. Chem., Int. Ed.* **2016**, *55*, 10376−10380.
(37) Lo, C. K.; Wang, C.-Y.; Oosterhout, S. D.; Zheng, Z.; Yi, X.; Fuentes-Hernandez, C.; So, F.; Coropceanu, V.; Brédas, J.-L.; Toney, M. F.; et al. Langmuir-Blodgett Thin Films of Diketopyrrolopyrrole-Based Amphiphiles. *ACS Appl. Mater. Interfaces* **2018**, *10*, 11995−12004.
(38) Yang, S.-F.; Liu, Z.-T.; Cai, Z.-X.; Dyson, M.-J.; Stingelin, N.; Chen, W.; Ju, H.-J.; Zhang, G.-X.; Zhang, D.-Q. Diketopyrrolopyrrole-Based Conjugated Polymer Entailing Triethylene Glycols as Side Chains with High Thin-Film Charge Mobility without Post-Treatments. *Adv. Sci.* **2017**, *4*, 1700048.
(39) Yang, S.-F.; Zhang, X.; Chen, P.-L.; Liu, Z.-T.; Tian, J.-W.; Zhang, G.-X.; Zhang, D.-Q. Diketopyrrolopyrrole-Based Semiconducting Polymer with Both Hydrophobic Alkyl and Hydrophilic Tetraethylene Glycol Chains for Monolayer Transistor and Sensing Application. *Adv. Electron. Mater.* **2017**, *3*, 1700120.
(40) Chang, W.-H.; Gao, J.; Dou, L.; Chen, C.-C.; Liu, Y.; Yang, Y. Side-Chain Tunability via Triple Component Random Copolymerization for Better Photovoltaic Polymers. *Adv. Energy Mater.* **2014**, *4*, 1300864.
(41) Lu, K.; Fang, J.; Zhu, X.; Yan, H.; Li, D.; Di, C. a.; Yang, Y.; Wei, Z. A Facile Strategy to Enhance the Fill Factor of Ternary Blend Solar Cells by Increasing Charge Carrier Mobility. *New J. Chem.* **2013**, *37*, 1728−1735.
(42) Meng, B.; Liu, J.; Wang, L. Oligo(Ethylene Glycol) as Side Chains of Conjugated Polymers for Optoelectronic Applications. *Polym. Chem.* **2020**, *11*, 1261−1270.
(43) Cardona, C. M.; Li, W.; Kaifer, A. E.; Stockdale, D.; Bazan, G. C. Electrochemical Considerations for Determining Absolute Frontier Orbital Energy Levels of Conjugated Polymers for Solar Cell Applications. *Adv. Mater.* **2011**, *23*, 2367−2371.
(44) Gross, Y. M.; Trefz, D.; DIngler, C.; Bauer, D.; Vijayakumar, V.; Untilova, V.; Biniek, L.; Brinkmann, M.; Ludwigs, S. From Isotropic to Anisotropic Conductivities in P(NDI2OD-T2) by (Electro-)Chemical Doping Strategies. *Chem. Mater.* **2019**, *31*, 3542−3555.
(45) Trefz, D.; Ruff, A.; Tkachov, R.; Wieland, M.; Goll, M.; Kiriy, A.; Ludwigs, S. Electrochemical Investigations of the N-Type Semiconducting Polymer P(NDI2OD-T2) and Its Monomer: New Insights in the Reduction Behavior. *J. Phys. Chem. C* **2015**, *119*, 22760−22771.
(46) Chen, Z.; Zheng, Y.; Yan, H.; Facchetti, A. Naphthalenedicarboximide- vs Perylenedicarboximide-Based Copolymers. Synthesis and Semiconducting Properties in Bottom-Gate N-Channel Organic Transistors. *J. Am. Chem. Soc.* **2009**, *131*, 8−9.
(47) Guo, X.; Kim, F. S.; Seger, M. J.; Jenekhe, S. A.; Watson, M. D. Naphthalene Diimide-Based Polymer Semiconductors: Synthesis, Structure−Property Correlations, and n-Channel and Ambipolar Field-E Ff Ect Transistors. *Chem. Mater.* **2012**, *24*, 1434−1442.
(48) Bredas, J. L.; Street, G. B. Polarons, Bipolarons, and Solitons in Conducting Polymers. *Acc. Chem. Res.* **1985**, *18*, 309−315.
(49) Lu, N.; Li, L.; Liu, M. A Review of Carrier Thermoelectric-Transport Theory in Organic Semiconductors. *Phys. Chem. Chem. Phys.* **2016**, *18*, 19503−19525.
(50) Bubnova, O.; Berggren, M.; Crispin, X. Tuning the Thermoelectric Properties of Conducting Polymers in an Electrochemical Transistor. *J. Am. Chem. Soc.* **2012**, *134*, 16456−16459.
(51) Hwang, S.; Potscavage, W. J.; Yang, Y. S.; Park, I. S.; Matsushima, T.; Adachi, C. Solution-Processed Organic Thermoelectric Materials Exhibiting Doping-Concentration-Dependent Polarity. *Phys. Chem. Chem. Phys.* **2016**, *18*, 29199−29207.
(52) Liu, J.; Qiu, L.; Portale, G.; Koopmans, M.; ten Brink, G.; Hummelen, J. C.; Koster, L. J. A. N-Type Organic Thermoelectrics: Improved Power Factor by Tailoring Host−Dopant Miscibility. *Adv. Mater.* **2017**, *29*, 1701641.
(53) Voortman, T. P.; Chiechi, R. C. Thin Films Formed from Conjugated Polymers with Ionic, Water-Soluble Backbones. *ACS Appl. Mater. Interfaces* **2015**, *7*, 28006−28012.
(54) Estrada, L. A.; Liu, D. Y.; Salazar, D. H.; Dyer, A. L.; Reynolds, J. R. Poly[Bis-EDOT-Isoindigo]: An Electroactive Polymer Applied to Electrochemical Supercapacitors. *Macromolecules* **2012**, *45*, 8211−8220.
(55) Liu, J.; Ye, G.; Potgieser, H. G. O.; Koopmans, M.; Sami, S.; Nugraha, M. I.; Villalva, D. R.; Sun, H.; Dong, J.; Yang, X.; et al. Amphipathic Side Chain of a Conjugated Polymer Optimizes Dopant Location toward Efficient N-Type Organic Thermoelectrics. *Adv. Mater.* **2021**, *33*, 2006694.

https://doi.org/10.1021/acs.macromol.1c00317
Macromolecules 2021, 54, 3886−3896